J Porous Mater (2012) 19:551–556
DOI 10.1007/s10934-011-9504-7

Thermal conductivity of low density carbon aerogels

Junzong Feng · Jian Feng · Changrui Zhang

Published online: 31 July 2011

Abstract Carbon aerogels with densities ranging from 0.182 to 0.052 g/cm^3, pore sizes ranging from 88 to 227 nm, and particle diameters ranging from 20 to 13 nm were prepared. Thermal conductivity measurements by laser flash method indicate that the lowest thermal conductivity can be obtained at a density of 0.066 g/cm^3, in the temperature range from 100 to 300 °C in air. The lowest thermal conductivity is 0.0263 W/m K at 200 °C. The characteristic density, at which the lowest thermal conductivity can be obtained, is temperature dependent. At a higher temperature, a higher density carbon aerogel will be more efficient in the reduction of the total conductivity by reducing the radiative conductivity.

Keywords Carbon aerogels · Thermal conductivity · Low density · Pore size

1 Introduction

Because of their excellent thermal insulation properties, nanostructured aerogels are promising materials for thermal insulators [1]. In all kinds of aerogels with various chemical components that have been explored to date, carbon aerogels (CAs) [2–5] have the highest thermal stability and can maintain their mesoporous nanostructure at a high temperature even exceed 2,000 °C in an inert atmosphere [6]. For comparison, the surface area of SiO_2–Al_2O_3 hybrid aerogels decreased sharply at above 1,300 °C [7]. In addition, the specific extinction coefficients of the CAs are much higher than those of other aerogels, e.g. 190 m^2/kg for CAs [8] and 20 m^2/kg for pure silica aerogels [1], thus the radiative thermal conduction transmitted through the CAs is very low [8]. These merits mentioned above make CAs to be the promising candidates for extreme applications such as the high temperature thermal insulations [9] for advanced industrial devices, space vehicles landing on other planets, and hypersonic vehicles, in which the heat flux and the temperature are extremely high and the weight and the thickness of the thermal insulation are strictly limited.

However, the thermal conductivities of aerogels are affected significantly by their densities. The smallest measured thermal conductivities were 0.012 W/m K at a density of 0.157 g/cm^3 for organic aerogels, and 0.013 W/m K at a density of 0.120 g/cm^3 for SiO_2 aerogels [1]. Lu et al. [10] had determined the thermal conductivities of CAs with densities ranging from 0.082 to 0.637 g/cm^3 at room temperature, and concluded that at a density of 0.082 g/cm^3, which is the lowest density limit in their experiments, the smallest thermal conductivity can be obtained. There was no experimental data evidence for a lower density CA. The lowest densities of CAs that other authors consequently prepared for thermal conductivity measurements were 0.381 [11], 0.301 [8], 0.240 [12], and 0.225 g/cm^3 [9], respectively. However, the solid thermal conductivity (λ_s) of nonporous carbon materials is higher than those of the nonporous organic or the oxide bulk materials, because of the strong bonding of the light carbon atoms resulting in a large phonon contribution to the thermal conductivity [13]. We surmise that the density, at

Electronic supplementary material The online version of this article (doi:10.1007/s10934-011-9504-7) contains supplementary material, which is available to authorized users.

J. Feng · J. Feng (✉) · C. Zhang
Key Lab of Advanced Ceramic Fibers and Composites, College of Aerospace and Materials Engineering, National University of Defense Technology, 109 De Ya Rd, Changsha 410073, Hunan, China
e-mail: fengj1277@sohu.com

which the smallest thermal conductivity can be obtained for CAs, would be lower than 0.082 g/cm^3 (in Ref. [10]). In order to verify our assumption, herein we introduce the fabrication of CAs with densities as low as 0.052 g/cm^3, and the first characterization of their thermal conductivities in the temperature range from 100 to 300 °C in air by laser flash method.

2 Experimental section

2.1 Preparation

Organic aerogels were synthesized by using resorcinol (R) and formaldehyde (F) as precursors, deionised water (W) as solvent, and sodium carbonate (C) as catalyst [14]. Five series of RF aerogels with various R/C and W/R molar ratios were prepared. The F/R molar ratio was two, the R/C and the W/R molar ratios were shown in Table 1. After mixing the raw materials in together and magnetically stirring for 30 min, the RF solutions were sealed in glass test tubes with 18 mm diameter, and kept at room temperature for 1 day, then gelled in 50 °C water bath for 1 day, and cured at 80 °C for 3 days. The obtained aquagel columns were soaked in ethanol for 3 days, then exchanged with petroleum ether (boiling point: 30–60 °C) for another 3 days, the ethanol and the petroleum ether were exchanged one time for each day. The gel columns were placed in an autoclave (volume: 3 L) and supercritically dried with petroleum ether (240 °C, 7 MPa). The obtained RF aerogel columns were carbonized at 1,000 °C for 1 h in a tube furnace with flowing nitrogen (100 mL/min) to form CAs.

2.2 Characterization

The bulk densities (ρ) of the CAs were obtained by measuring the volumes and the weights of the aerogel columns. Nitrogen sorption measurements were performed to obtain pore properties such as the BET-specific surface area (S_{BET}) and the external specific surface area (S_{ext}, i.e. surface area including mesopore and macropore) with a QuadraSorb SI (Quantachrome, USA) analyzer. S_{ext} was calculated by t-plot method. The mean pore size (D_{pore}) was calculated by Eq. 1 [9, 12], and mean particle diameter ($d_{particle}$) by Eq. 2 [9, 12].

$$D_{pore} = \frac{4}{S_{ext}}\left(\frac{1}{\rho} - \frac{1}{\rho_s}\right) \quad (1)$$

$$d_{particle} = \frac{6}{S_{ext}\rho_s} \quad (2)$$

S_{ext} is the external surface area. ρ is the bulk density of the aerogel samples, and ρ_s is the intrinsic density of the backbone particles formed the the aerogels, ρ_s = 1,400 kg/m^3 [9, 12].

The morphologies of the CAs were investigated by Hitachi S4800 (Japan) scanning electron microscope (SEM) after coating with a thin platinum layer. The CA columns (Online Resource Fig. s1) were carefully cut into disk-shape with diameters of 12.7 mm and thicknesses of approximately 1.3 mm (as shown in Fig. 1) by an automatic diamond saw device with a low moving speed of 1 mm/min, and the thermal diffusivities of the disk-shape samples were determined by the laser flash method in air, using a Netzsch LFA 447 (German) apparatus. We found that, in the relatively low temperature range from 25 to 70 °C, the thermal diffusivities were much higher than the values in the temperature range above 100 °C, especially for the lower density CA (Online Resource Fig. s2). The

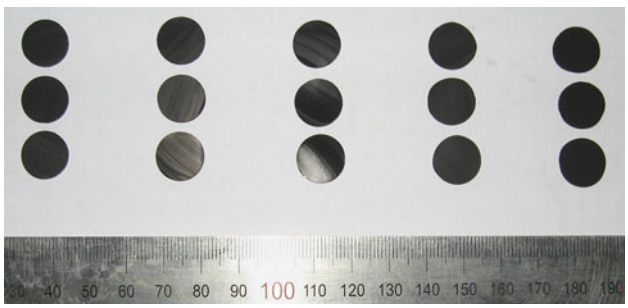

Fig. 1 The CA specimens with diameters of 12.7 mm and thicknesses of approximately 1.3 mm for the laser flash measurements. From *left to right*: 0.182, 0.128, 0.097, 0.066, 0.052 g/cm^3, respectively

Table 1 The linear shrinkage and the textural properties of the RF aerogels and the CAs

Series	R/C	W/R	Shrinkage during drying (%)	RF aerogel density (g/cm^3)	Shrinkage during pyrolysis (%)	Carbon yield (%)	CA density (g/cm^3)	S_{BET} (m^2/g)	S_{ext} (m^2/g)	D_{pore} (nm)	$d_{particle}$ (nm)
1	546	44	6.7	0.168	24.0	49.5	0.182	545	218	88	20
2	500	64	5.6	0.119	24.5	48.6	0.128	561	250	113	17
3	455	89	5.0	0.091	24.5	47.9	0.097	537	226	170	19
4	417	128	5.5	0.063	24.9	47.2	0.066	563	289	200	15
5	357	177	2.0	0.047	25.9	46.9	0.052	666	329	227	13

reason may be that the adsorption of water and gas molecules enhanced the gas thermal transport. Therefore, to minimize the effects of the adsorbed water and other gas molecules, the measurement were performed under the temperature range from 100 to 300 °C. The Cowan method was selected to correct the diffusivity measurements. The total thermal conductivity $\lambda_t(T)$ was obtained according to Eq. 3 from the thermal diffusivity $\alpha(T)$, with the specific heat capacity $c_p(T)$ and the density ρ [9].

$$\lambda_t(T) = \alpha(T)\rho c_p(T) \quad (3)$$

T is the temperature at which the measurement was performed. Literature values of $c_p(T)$ were used [9]. Standard deviation error for the thermal conductivity measurement was estimated to be 15%.

3 Results and discussion

3.1 Textural properties of the aerogels

Table 1 shows the linear shrinkage and the textural properties of the RF aerogels and the CAs during the synthesizing process. During the supercritical drying process, only a relatively low linear shrinkage (2–6.7%) occurs, the linear shrinkage decreases mildly with increasing the W/R value, due to the larger pore size and thus induces lower capillary pressure in the higher W/R value gels. Relatively large linear shrinkage (24–25.9%) occurs during the carbonization process, regardless of the R/C values or the W/R values. With the designed variation of W/R values from 44 to 177, the density of the CAs decreases from 0.182 to 0.052 g/cm^3, which is exceeded the lowest density limit (0.082 g/cm^3) in Ref. [10]. The S_{BET} and the S_{ext} of the CAs, obtained by nitrogen sorption analysis (the nitrogen sorption isotherms are shown in Fig. 2), are not changed obviously with the variation of R/C and W/R values. The $d_{particle}$, affected mostly by the R/C value [2, 4], decreases mildly from 20 to 13 nm, with the decreasing of R/C values from 546 to 357. The D_{pore}, affected mostly by the W/R value [2, 4], increases from 88 to 227 nm, with the increasing of W/R values from 44 to 177. The D_{pore} is comparable to the mean free path of air ($\approx$70 nm at room temperature) [1], it indicates that the Knudsen number (Kn) is of the order of 1 and the thermal transport is semi-ballistic, which is important in nanoscale heat transfer [15].

Figure 3 shows the SEM images of the CAs with different densities. The CAs are three dimension network nanostructures formed by pearl-necklace chains. The structure of the CAs with lower density is looser and the pore diameter is larger than the one with higher density, but the $d_{particle}$ which formed the network is not changed. The

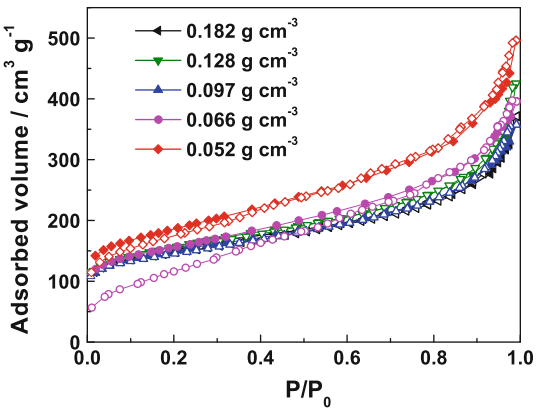

Fig. 2 The nitrogen sorption isotherms of the CAs with various densities

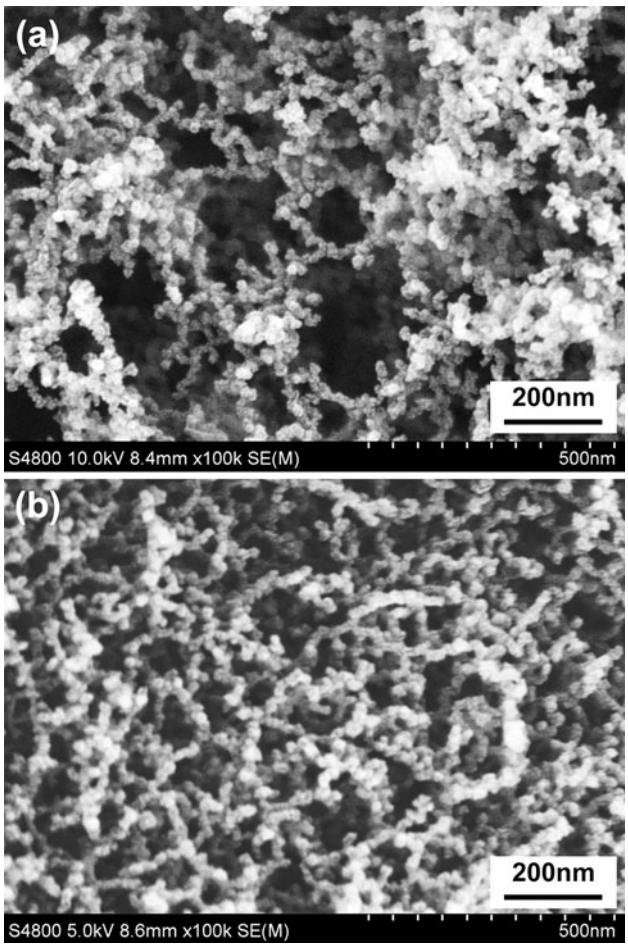

Fig. 3 SEM images of the low density CAs with various densities. **a** 0.052 g/cm^3. **b** 0.182 g/cm^3

$d_{particle}$ is approximately 20 nm, this size is consistent with the data in Table 1. The porosity decreases as the density increases (W/R value decreases). This indicates that the gaseous thermal conductivity will decrease as the W/R value decreases.

3.2 Thermal conductivities of the aerogels

Figure 4 shows the thermal diffusivities of the CAs with various densities at the temperatures ranging from 100 to 300 °C in air. The thermal diffusivities measured at the relatively low temperature range from 25 to 70 °C are much higher than the values measured at the temperature range above 100 °C, especially for the lower density CA (Online Resource Fig. s2). This phenomena may be attributed to the adsorption of water and gas molecules on the nanostructured network of the CAs. This adsorption can be classified into two mechanisms: chemisorption and physisorption. The chemisorption of gas molecules may decrease the surface energy of the solid backbone of the CA and thus decrease the solid conductivity [16, 17]. But the chemisorption can not be vented out when it is heated up to a relatively low temperature (100 °C), thus the higher thermal diffusivity in the relatively low temperature (25–70 °C) may be attributed to the physisorption, which is desorbed when it is heated up to 100 °C. The physisorption of gas molecules in the nanopores of the CA will increase the possibilities of collisions between the gas molecules and thus increase the gaseous conductivity [18]. For the lower density CA, the pore size is larger and thus the gaseous conductivity is higher than that of the CA with higher density. Therefore, the physisorption of gas molecules shows more significant effects on the thermal diffusivity in a low density CA than in a high density one. To minimize the effects of physisorption, only the thermal diffusivities in the temperature range from 100 to 300 °C are used to calculate the thermal conductivities (Fig. 4). For the higher density (0.097–0.182 g/cm^3) CAs, the thermal diffusivities is almost constant with increasing the temperature. While for the relatively lower density (0.052–0.066 g/cm^3) CAs, the thermal diffusivities increase with increasing the temperature, especially for the CAs with the lowest density (0.052 g/cm^3). At a certain temperature, the thermal diffusivities increase with decreasing the CA densities.

Figure 5 shows the $\lambda_t(T)$ of CAs with various densities versus measuring temperature in air. The $\lambda_t(T)$ of CA with the highest density (0.182 g/cm^3) is the highest in the whole temperature range, because of its relatively high solid conductivity $\lambda_s(T)$. For the CA with the lowest density (0.052 g/cm^3), the $\lambda_t(T)$ increases much more rapidly with temperature, than those of other CAs. This indicates that the radiative conductivity $\lambda_r(T)$ contributes a large component in the $\lambda_t(T)$. Because the $\lambda_r(T)$ is proportional to the reciprocal of density ($1/\rho$), the lower the density, the higher the $\lambda_r(T)$.

The $\lambda_r(T)$ of the aerogel can be described by [1, 12]

$$\lambda_r(T) = \frac{16n^2\sigma_B}{3\rho e(T)}T^3 = \frac{R(T)}{\rho} \quad (4)$$

where n is the mean index of refraction, $n = 1.1$ for carbon aerogel [12]. σ_B is the Stefan-Boltzmann constant. $e(T)$ is the specific extinction coefficient. Because the $d_{particle}$ is not changed too much for CAs with various densities in this present work, the $e(T)$ is estimated to be the same. Thus, at a certain temperature T, the $\lambda_r(T)$ can be simplified as $R(T)/\rho$. $R(T)$ is the fit parameter.

The $\lambda_s(T)$ of low density aerogel can be written as [1, 8]

$$\lambda_s(T) = C(T)\rho^{1.5} \quad (5)$$

where $C(T)$ is the fit parameter.

The gaseous conductivity $\lambda_g(T)$ can be described as [1, 12]

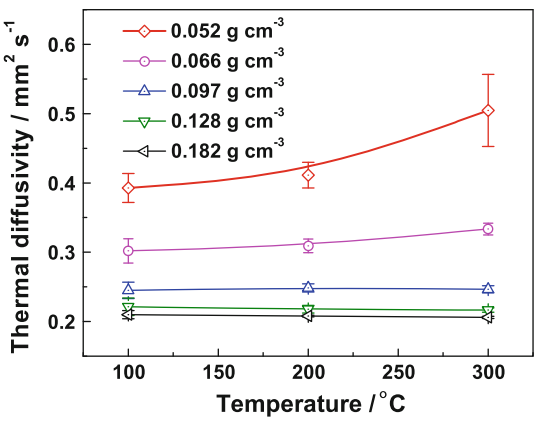

Fig. 4 Thermal diffusivities of the CAs with various densities under various temperatures in air. The *error bars* indicate the standard error of twelve results of three specimens, with four flash pulses for each specimen

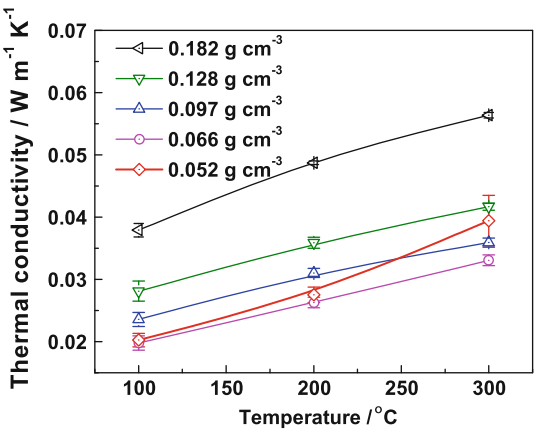

Fig. 5 Total thermal conductivities of the CAs with various densities versus measuring temperature in air. The *error bars* indicate the standard error of twelve experimental results of three specimens, with four flash pulses for each specimen. The *solid lines* are guides to the eye

$$\lambda_g(T) = \frac{\Pi\lambda_{g0}(T)}{1+\beta Kn} \tag{6}$$

where Π is the porosity calculated by

$$\Pi = 1 - \frac{\rho}{\rho_s} \tag{7}$$

where ρ_s is the density of the carbon particles, $\rho_s = 1{,}400$ kg/m^3 [12]. $\lambda_{g0}(T)$ is the gaseous conductivity of a free gas. In air, $\lambda_{s0}(300\ ^\circ\text{C})$ is approximately 0.045 W/m K. $\beta \approx 2$ for air in aerogel [1]. The Knudsen number is

$$Kn = \frac{l_g(T)}{D_{\text{pore}}} \tag{8}$$

where $l_g(T)$ describes the mean free path of the gas particles, and is a function of the temperature according to Eq. 9 [12]. $l_g(300\ ^\circ\text{C})$ is approximately 110 nm for air.

$$l_g(T) = \frac{k_B T}{\sqrt{2\sigma_0 p_g}} \tag{9}$$

To calculate the Kn for CAs with various densities, the D_{pore} is obtained by fitting the experimental D_{pore} data with an exponential function as

$$D_{\text{pore}} = A \times \exp\left(-\frac{\rho}{t}\right) \tag{10}$$

A and t is the fit parameters. The fitting results are shown in Fig. 6.

The total thermal conductivity of CA thus becomes

$$\begin{aligned}\lambda_t(T) &= \lambda_r(T) + \lambda_s(T) + \lambda_g(T) \\ &= R(T)\rho^{-1} + C(T)\rho^{1.5} + \lambda_g(T).\end{aligned} \tag{11}$$

The relationships between the $\lambda_t(T)$ and the densities of the CAs and their fitting lines by Eq. 11 are shown in Fig. 7. With the decreasing of the density from 0.182 to 0.066 g/cm^3, the $\lambda_t(T)$ decreases significantly and shows a strong density-dependence relationship. When the density continues to decrease from 0.066 to 0.052 g/cm^3, the $\lambda_t(T)$ of the CAs increases, especially for the values at 300 °C. This gives a concrete evidence for that the lowest $\lambda_t(T)$ can be obtained at a density of 0.066 g/cm^3. Because when the density is lower than 0.066 g/cm^3, the $\lambda_r(T)$ will increase rapidly and contributes a large component into the $\lambda_t(T)$. The smallest thermal conductivity is 0.0263 W/m K at 200 °C. This value is lower than the value (0.029 W/m K) for a CA with a density of 0.082 g/cm^3 in air at room temperature in Ref. [10]. We consider that the reason may be the lower density in our CA and the prevention of the effects of adsorbed gas molecules in our measurements. From the fitting line in Fig. 7 for various temperatures, it can be seen that the characteristic density, at which the smallest thermal conductivity can be obtained, increases when the temperature increases. Because the $\lambda_r(T)$ is proportional to three power of temperature (T^3), as the temperature increases, the $\lambda_r(T)$ increases more rapidly than the $\lambda_s(T)$ or the $\lambda_g(T)$. Thus a higher density will be more efficient in reducing the $\lambda_r(T)$ at high temperature and results in reduction in the $\lambda_t(T)$.

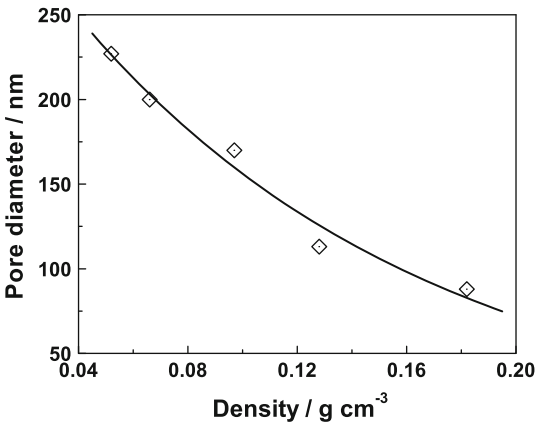

Fig. 6 Pore sizes of the CAs versus their densities. The *solid line* is the fitting result of the experimental data (*open diamond*) with Eq. 10

4 Conclusion

We prepared CAs with density as low as 0.052 g/cm^3. Thermal conductivity measurements indicate that the lowest thermal conductivity can be obtained at a density of 0.066 g/cm^3 for CAs in the temperature range from 100 to 300 °C. The characteristic density, at which the smallest thermal conductivity can be obtained, is temperature dependent. At higher temperature, higher density CAs will be more efficient in the reduction of the $\lambda_t(T)$ by reducing the $\lambda_r(T)$. Therefore, one should consider the working

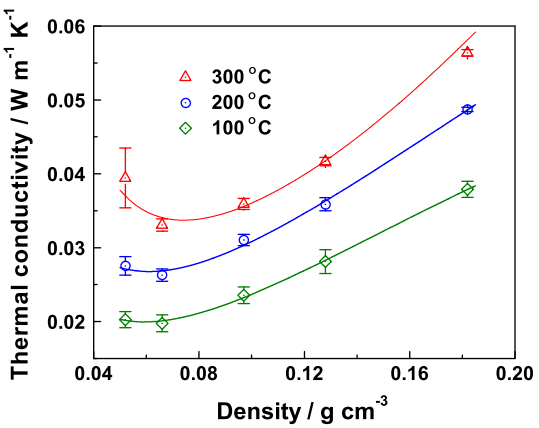

Fig. 7 Total thermal conductivities of the CAs versus their densities under various temperatures in air. The *error bars* indicate the standard error of twelve experimental results of three specimens, with four flash pulses for each specimen. The *solid lines* are the fitting results of the experimental data with Eq. 11

temperature of the given environment to design the density of the CAs for thermal insulation applications.

Acknowledgments The authors gratefully acknowledge financial supports from National Natural Science Foundation (51002187) and National Defense Preliminary Research Foundation (9140C820 3051003) of China. Dr. Yonggang Jiang is thanked for helpful discussions and comments. The authors would also like to thank Dr. Shun Li and Dr. Meng Liu for the laser flash measurements.

References

1. X. Lu, M.C. Arduini-Schuster, J. Kuhn, O. Nilsson, J. Fricke, R.W. Pekala, Science **255**, 971 (1992)
2. S.A. Al-Muhtaseb, J.A. Ritter, Adv. Mater. **15**, 101 (2003)
3. D. Wu, R. Fu, J. Porous Mater. **15**, 29 (2008)
4. M. Mirzaeian, P.J. Hall, J. Mater. Sci. **44**, 2705 (2009)
5. C. Scherdel, R. Gayer, T. Slawik, G. Reichenauer, T. Scherb, J. Porous Mater. **18**, 443 (2011)
6. Y. Hanzawa, H. Hatori, N. Yoshizawa, Y. Yamada, Carbon **40**, 575 (2002)
7. T. Horiuchi, T. Osaki, T. Sugiyama, K. Suzuki, T. Mori, J. Non-Cryst. Solids **291**, 187 (2001)
8. M. Wiener, G. Reichenauer, F. Hemberger, H.P. Ebert, Int. J. Thermophys. **27**, 1826 (2006)
9. M. Wiener, G. Reichenauer, S. Braxmeier, F. Hemberger, H.P. Ebert, Int. J. Thermophys. **30**, 1372 (2009)
10. X. Lu, O. Nilsson, J. Fricke, R.W. Pekala, J. Appl. Phys. **73**, 581 (1993)
11. V. Bock, O. Nilsson, J. Blumm, J. Fricke, J. Non-Cryst. Solids **185**, 233 (1995)
12. F. Hemberger, S. Weis, G. Reichenauer, H.P. Ebert, Int. J. Thermophys. **30**, 1357 (2009)
13. J.H. Seol, I. Jo, A.L. Moore, L. Lindsay, Z.H. Aitken, M.T. Pettes, X. Li, Z. Yao, R. Huang, D. Broido, N. Mingo, R.S. Ruoff, L. Shi, Science **328**, 213 (2010)
14. R.W. Pekala, J. Mater. Sci. **24**, 3221 (1989)
15. R. Carminati, *Microscale and Nanoscale Heat Transfer, Topics in Applied Physics*, Vol. 107. ed. by S. Volz (Springer-Verlag, Berlin Heidelberg, 2007), pp. 15–35
16. R. Prasher, Phys. Rev. B **74**, 165413 (2006)
17. C.W. Padgett, D.W. Brenner, Nano Lett. **4**, 1051 (2004)
18. W.D. Zhou, B. Liu, S.K. Yu, W. Hua, Phys. Rev. E **81**, 011204 (2010)